Chapter 3

Novel Ganga-sand-encapsulated polyaniline granules for effective remediation of textile and pharmaceutical wastewater

3.1 Introduction

Wastewater generated due to use of synthetic dyes causes severe effect on the environment and water sources so need to treated properly before release. The exiting option available for toxic dye wastewater treatment insufficient because vigorous increase in toxic dye wastewater generated from various industries multiplied Calimli et al. (2020). It has become severe problem for public health and environment. Continuous discharge of industrial dye waste water into water sources endangers human health and the environment, Othman et al. (2018). The disposal of untreated dye-containing effluent into in water sources affect ecosystems of aquatic life and photosynthetic action, Ahmed et al. (2018). Furthermore, accumulation of antibiotic in the environment become the key issue of concern to the scientists and environmentalists Bai et al. (2018). Even at low-level with long-time exposure of antibiotics lead to adverse impact such as hypersensitive responses, abnormalities in digestive system working, allergic responses to the microbes, Khan et al. (2022). Moreover, small traces of antibiotics in the environment causes enduring toxicity to organisms in long duration. Release of antibiotics in the environment leads to the growth of antibiotic-resistant microorganisms adversely effect to the human well-being by endocrine interruption, upsurge of antibiotic resistance species and the potentially ill effects of their undesirable/unidentified by products, Huang et al. (2019).

Methylene Blue (MB) is the most used dyes in textile industries. However, it imparts many risks to human health for example abdominal disorders, respiratory distress, diarrhoea, vomiting, cyanosis, blindness, digestive, mental disorders. Moreover, its exposure to skin causes skin redness and itching. Doxycycline is broad spectrum antibiotics which used for treat different infections like acne, urinary tract infections, respiratory infections, intestinal infections, eye infections, gonorrhoea, chlamydia, syphilis, periodontitis (gum disease), and many types,(Ghaemi and Absalan, 2014). Doxycycline (DXN) is a broad-spectrum

antibacterial drug consisting of free -OH, -NH_2 and carbonyl groups, Hasanova (2021). Hence, it is used frequently and therefore its accumulation value is high in the water resources due to unrestricted discharges, Wei et al. (2019). Recent years have seen an increase in cases where antibiotics have been found in water and the danger that comes with it.

The conventional options available applied for the reduction of antibiotics from wastewater systems may need further improvement, Ali and Ahmed (2017). Many options stated designed for the treatment of antibiotics (advanced oxidation, ozonation, membrane filtration, reverse osmosis, electrochemical methods, and biological treatments), Saxena et al. (2022). Many of these methods are not economical and produces by product which make them less effective Xu et al. (2021). Many options available for treatment of treatment to the wastewater of antibiotics and dyes but we prefer adsorption because adsorption technologies construction assembly simple design, operation is easy and low cost compare to others, Zaidi et al. (2016). Recently, varied types of adsorbent materials have been developed for specific chemical system and low-cost waste material-based adsorbents with polymer provide improved option. Polyaniline sand composite synthesise by simple in situ oxidation reaction of aniline with sand using potassium chromate ($K_2Cr_2O_7$) as an oxidizing agent was presented by Yu et al. (2021). The adsorption capability of M-CN/ cLDH (calcined layered double hydroxide composite) was ascribed to the superior adsorption capacity of the cLDH layered component and the outstanding photocatalytic action originated from the exclusive micro-morphology and the CN-cLDH heterojunctions. There have been several studies based on composites for removal of DXN antibiotic from wastewater. Aniagor et al. (2021), synthesised hierarchical $CoFe_2O_4$/bio-silica nanocomposite for removal of DXN antibiotic. They found highest adsorption capacity of 835.45 mg/g for removal of DXN from wastewater. Ali et al. Ali and Ahmed (2017), prepared NaY zeolite with could be an efficient adsorbent for treatment of antibiotic impurities in wastewaters. Rahman and Varshney (2021), synthesized CuO

nanoparticles decorated poly(2-acrylamido-2-methyl-1- propane sulfonic acid)/chitosan to explore its potential treatment of DXN from wastewater. Wei et al. (2019), loaded sludge biochar with a simple and inexpensive one-step amendment hydrothermal technique to treat wastewater. Zeng et al. (2018), advised that biochar formed at high temperature (i.e., 700 °C), has higher adsorption capacity for the adsorption of antibiotics than lower-temperature (i.e. 300 to 500 °C) biochar. Xiong et al. (2019), tried DXN removal from Ni-doped MIL-53(Fe) nanoparticles with better adsorption actions and good potency in aqueous system. Abdulsahib et al. (2020), prepared a GO/PVP-AAc hydrogel composite used for DXN adsorption on the surface through physical adsorption. There have been several studies based on composites for removal of methylene blue (MB) dye. Calimli et al. (2020), developed to remove MB dye using graphene-oxide-supported Ni nano adsorbents (Ni@rGO). Othman et al. (2018), synthesized graphene oxide- magnetic iron oxide nanoparticles and performed batch adsorption experiments with varied MB dye concentration, pH solution, adsorbent dosage besides contact time. M. Khan et al. (2022), established that improved surface polymers are more reactive for the elimination of dyes from waste water and have outstanding dye removal abilities in the wastewater treatment. Mor et al. (2017), synthesized economical and effective fly ash for the removal of MB dye from synthetic aqueous solution made adsorbent for the treatment of wastewater discharged from textile industries. Kara et al. (2021), synthesized sodium periodate-modified nanocellulose ($NaIO_4$-NC) from Eichhornia crassipes for the removal of cationic MB dye from wastewater. Ramutshatsha-Makhwedzha et al. (2022), prepared low-cost biosorbent orange and lemon peels-derived activated carbon that was effectively exploited in eliminating methyl orange and MB dyes from effluent. Ashik et al. (2023), used batch method for study of adsorption of MB in aqueous solution using coconut coir dust adsorbent. The present chapter focuses on elimination of MB dye and DXN antibiotic from the aqueous system. In this chapter, we use PANI impregnated sand adsorbent which is cost effective. PANI

based composite material withstand on extreme physiochemical condition and reusability make economical.

3.2 Material and methods

3.2.1 Materials

The sand samples were taken from the bank of river Ganga in Varanasi (India). The collected sand samples consisted of mineral and rocky particles, silt, and organic matter. It was cleaned with distilled water to remove dirt and soluble material and kept in an oven overnight for drying. The sand was treated with dilute HCl, washed and dried before using it for making the composite. Methylene Blue purchased from SD Fine chemicals (India).

3.2.2 Preparation of GS/PANI composite material

The sand was cleaned with distilled water and soaked in diluted HCl to eliminate any adhered leachable materials Gautam et al. (2017). The sand was heated at 400 °C in a muffle furnace to remove moisture and volatile organic matter. Dried and cleaned 10 g GS was soaked in 1 ml aniline and mixed to 0.1 N diluted HCl under vigorous stirring. 1 ml dilute solution of oxidizing agent ($K_2Cr_2O_7$) was added drop wise into the reaction vessel for initiating polymerization of aniline. The reaction mixture was kept at low temperature and continuously stirred for two hours. Green colour polymer was formed and deposited over sand particles Gautam et al. (2018). The reaction vessel was kept undisturbed for 24 hours for digestion followed by filtration, washing, and drying of the composite material. Initially the polymer formed was green in colour (as emaraldine salt formed). However, after washing with dilute water it converted into blue colour emaraldine or leucoemarldine base form. We observed that the sand had whitish and brownish colour whereas the composite material was dark blue in colour. Flow chart for composite preparation is given in Figure 3.1.

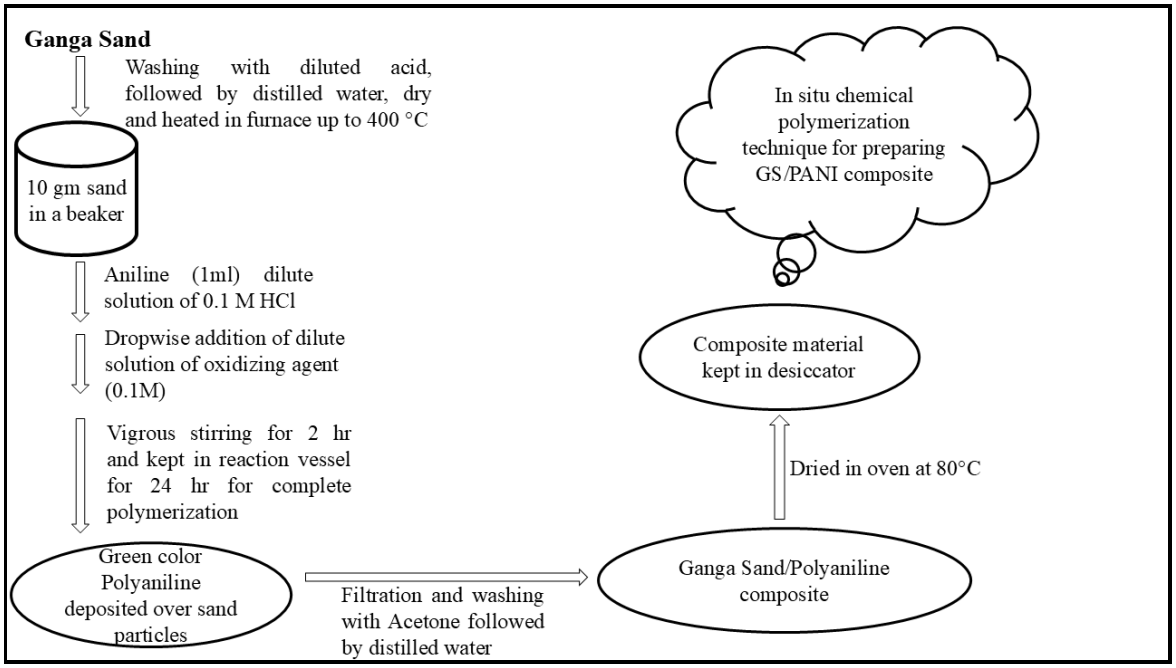

Figure 3.1 Preparation flow chart of GS/PANI composite material

3.3 Batch Adsorption experiment

Adsorption experiments were performed to examine effective removal MB dye and DXN antibiotic and adsorption capacity by means of GS/PANI composite material. A set of experiments were performed by altering various parameters like pH, adsorbent dosage, contact time to arrive at the optimum environments for the adsorption of MB dye and DXN antibiotic. To measure the effect of MB dye and DXN antibiotic concentration on the GS/PANI composite material, the concentration of solution was changed from 10 to 120 ppm. The pH of MB dye and DXN antibiotic solutions was changed from 2 to 12 to measure the effect caused by pH on MB dye and DXN antibiotic adsorption by GS/PANI composite material. The pH adjustment was achieved using 0.1 N HCl or 0.1 N NaOH for all the experiments. The initial adsorbent dose was changed from 0-12 mg/L to measure the effect caused by adsorbent dose on MB dye and DXN antibiotic adsorption by GS/PANI composite material. To improve the adsorption time, the adsorbents contact time was changed in the range of 10 to 180 min. Hence adsorption capacity as well as removal efficiency were assessed from the equations.

$$\text{Adsorption capacity } (q_e) = (C_i - C_e/m) \times V \quad (3.1)$$

The adsorbent was separated from the solution by using the Whatman filter paper. Maximum absorbance wavelength was identified for methylene blue dye and DXN antibiotic by scanning the absorbance from 200 nm to 800 nm using UV-visible spectrophotometer in the visible range. Dye and antibiotic concentration were measured at λ_{max} (668 nm for methylene blue and 362 nm for DXN using a UV-vis spectrophotometer. The following formula calculates the % removal of dye/antibiotic from dye/antibiotic solution. Initial absorption (initial dye solution) and final absorption (solution obtained after adsorption).

$$\text{Removal Efficiency} = (C_i - C_e / C_i) \times 100 \quad (3.2)$$

where q_e - equilibrium adsorption capacity, C_i - MB dye and DXN antibiotic primary concentration, C_e - MB dye and DXN antibiotic equilibrium concentration, m - mass of the sugarcane bagasse, and V - volume of MB dye and DXN antibiotic solution.

3.4 Adsorption kinetics

At the beginning of the adsorption, the process modifies as time goes forward. Therefore, time is important in learning kinetics of an adsorbent's performance Kurniawati et al. (2021). The pathway which is followed during the adsorption process can be predicted by studying the kinetics of the process. In the adsorption process, the physiochemical features of the adsorbent and system parameters such as contact time determines the nature and pathway of the process. The quantity of dye adsorbed at time t, denoted by q_t calculated by using the given equation:

$$q_t = (C_i - C_e / C_i) \times V \quad (3.3)$$

where q_t - adsorbed ions amount per unit mass of the adsorbent in time t, m - mass of adsorbent utilized, and C_t - contaminant's concentration at instant t. To examine the adsorption kinetics in this study, the linear pseudo-first-order (PFO) and the pseudo-second-order (PSO) kinetic models. The linear form of the PFO and PSO equation as given, Lin and Wang (2009), Sahu et al. (2019).

$$\ln (q_e - q_t) = \ln q_e - k_1 t \quad (3.4)$$

$$t/q_t = 1/k_2 q_e^2 + (1/ q_e) t \quad (3.5)$$

where q_t - amount of adsorbed ions per unit adsorbent at instant t, k_1-PFO constant, and k_2 - rate constant of the PSO.

Adsorption isotherm

The adsorption isotherms were utilized to examine the adsorption mechanism. The adsorption isotherms offer the equilibrium concentration between the adsorbed and unabsorbed phase at a specific state. Moreover, it helps to choose the adsorbents (Mate and Mishra (2020), Fakher and Imqam (2019). The Langmuir and Freundlich isotherms were select for this study. The Langmuir adsorption (monolayer adsorption) isotherm assumes that the adsorption occurs within the adsorbent at specific homogeneous positions. The linear form of the Langmuir isotherm is defined as:

$$C_e/ q_e = 1/ q_m K_L + (1/ q_m) C_e \quad (3.6)$$

where b - constant for Langmuir isotherm, q_m - maximum adsorption capacity, C_e - equilibrium concentration of dye in solution. The interaction as reversible and non-ideal adsorption is characterized by Freundlich isotherm. This isotherm model describes the adsorption process are multilayer sorption procedure of ions that bind on the surface of a heterogeneous adsorbent,

exponential distribution of active sites and energy onto the adsorbent surface. The linear type of the equation of Freundlich isotherm is defined as:

$$\ln q_e = \ln K_F + 1/n \quad \ln C_e \qquad (3.7)$$

where *n*- intensity and K_F - Freundlich coefficient.

3.5 Results and discussion

Functional and morphological characteristics govern the suitability of a material to act as an efficient adsorbent. We characterized GS and GS modified with PANI by FTIR, XRD, SEM, mesh size distribution of particles, optical microscopic images, and elemental analysis (C, H, N). Batch adsorption trials were performed to optimize the adsorption procedure for maximum removal of dye and antibiotic by prepared composite.

3.5.1 Grain size distribution of Ganga sand

The samples of the sand were randomly collected from many sand heaps made by the sand contractors and may be regarded as representative. The sieve analysis is graphically represented in the Figure 3.2. The quantity of mica by weight is quite small; its presence may give some elastic properties to the sand mass and influence compaction and shear strength. Very small size particles, dust and soluble materials were removed from the sand while washing with distilled water.

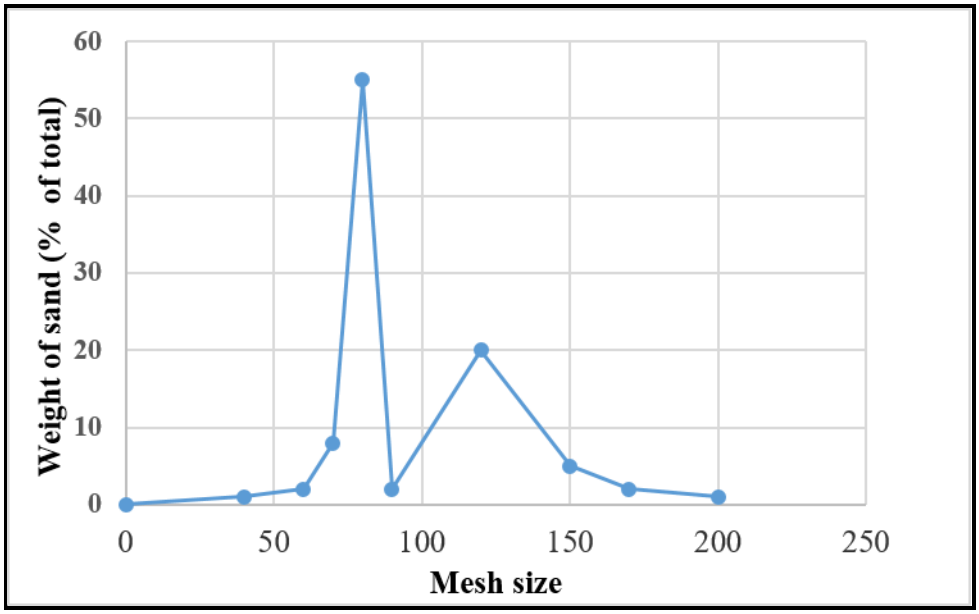

Figure 3.2 Distribution of sand particles based on different mesh size

3.5.2 Optical microscopic image of GS and GS/PANI composite material

An optical microscope was used at low magnification micrographs to determine the shape and size of sand grains and sand composite (Figure 3.3). Optical microscopic images reveal its morphology and texture, shape and size. The grain size of GS particles used in our work is less than 0.5 mm. GS grains have irregular and non-porous rough surface. We observed the grain boundary, texture, and colour from optical microscope images in plane and plane polarized light at magnification (Figure 3.4). The optical image of GS particle in plane and plane polarized light indicated that GS particles have rough surface texture, variable shape and size and multiple colours. Sand contains various minerals (primarily indicated from particles of differently coloured rocky particles. Sand grains of specific mineral species were not separately analysed in this paper for size and sphericity using this method; quartz grains strongly dominated in sand (shown in brilliant colours in plane polarized light along with other mineral grains).

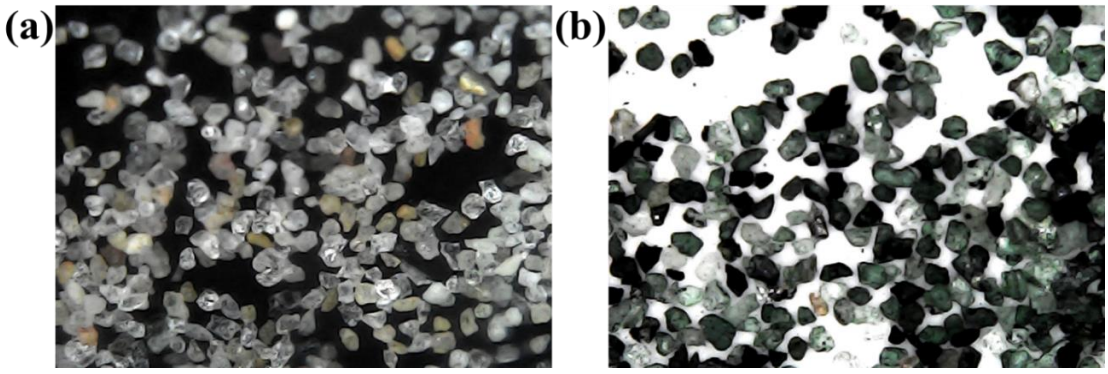

Figure 3.3 (a) Pristine GS and **(b)** PANI coated GS

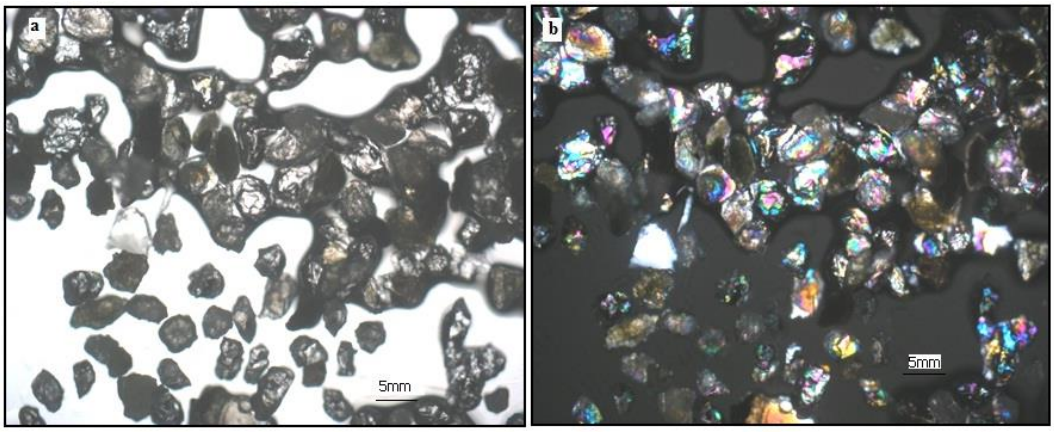

Figure 3.4 Optical images of **(a)** GS in plane light**, (b)** plane polarized light

Analysis of surface of sand grains before and after modification by PANI, at higher magnification (shown in Figure 3.5), revealed that polymer deposited as nano to micro sized island-like structures seems as dark spots, preferentially accumulating over rough portions, graves and cracks present over sand particles. The polymer fibres GS/PANI composite has compact and rough morphology and polymer modification increases the surface area and roughness of the sand particle. It is believed that PANI over sand particles provides additional adsorption sites for dye molecules and induce functionality over sand particles.

The energy dispersive X-ray spectroscopy (EDS) was performed to determine the elements in PANI and GS/PANI composite. As per the EDS results, the elements present in

PANI were Carbon and Nitrogen in the ratio of 56 wt.% and 44 wt.%, respectively (Figure 3.6). Further, as per the EDS results, the elements present in GS/PANI composite were Carbon, Nitrogen, oxygen, aluminium and silicon in the ratio of 40 wt.%, 2 wt.%, 38 wt.%, 2 wt.%, and 18 wt.% respectively (Figure 3.7).

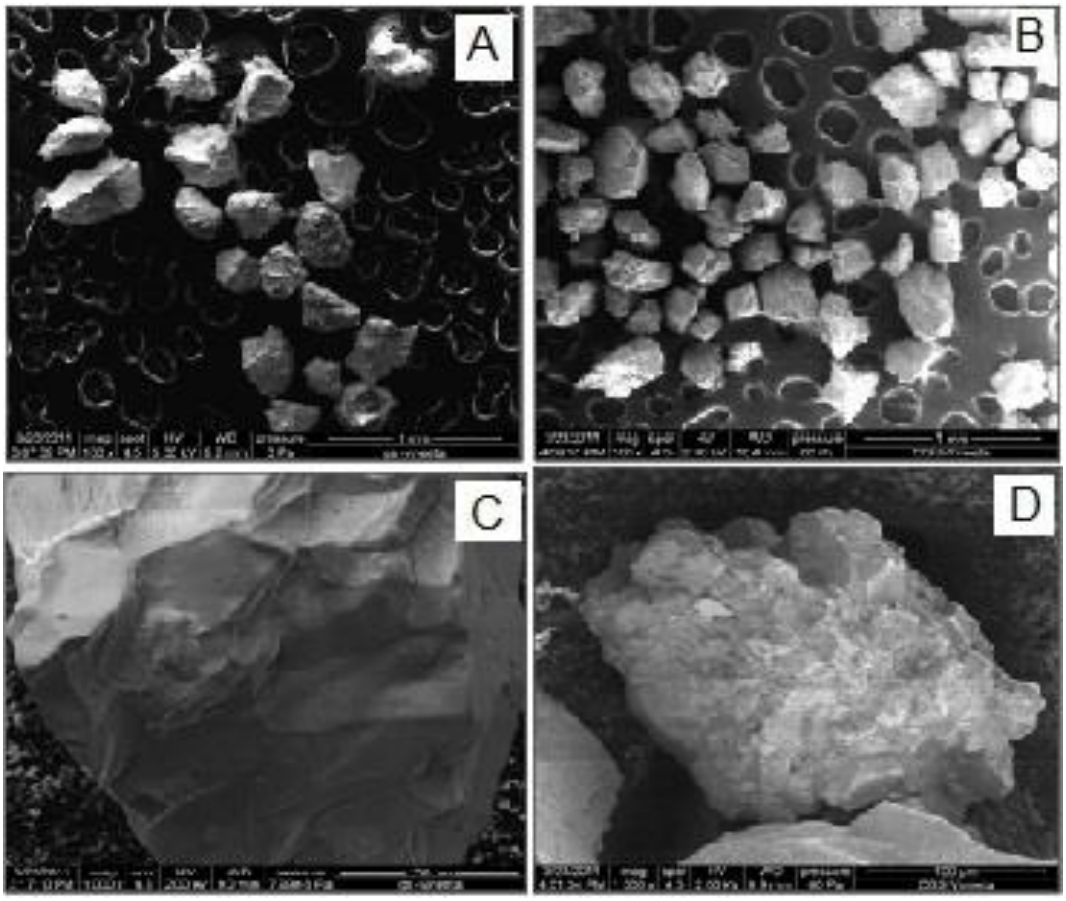

Figure 3.5 SEM image of GS particle

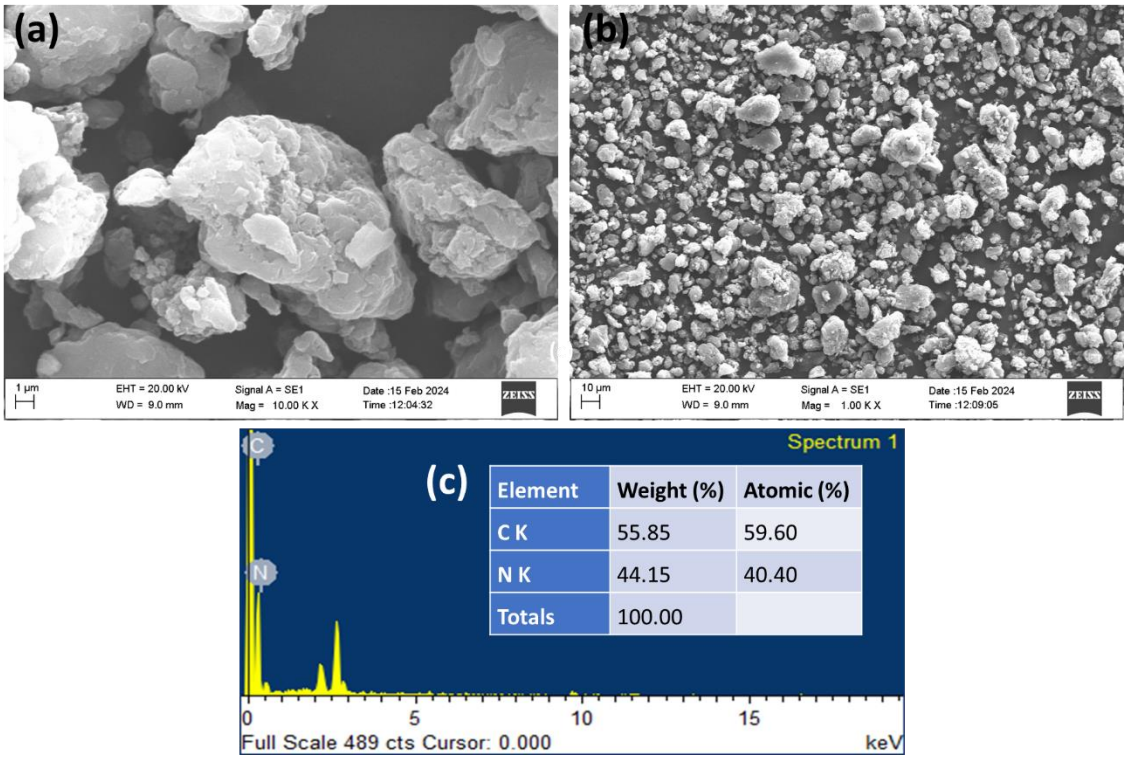

Figure 3.6 SEM image and EDAX of PANI

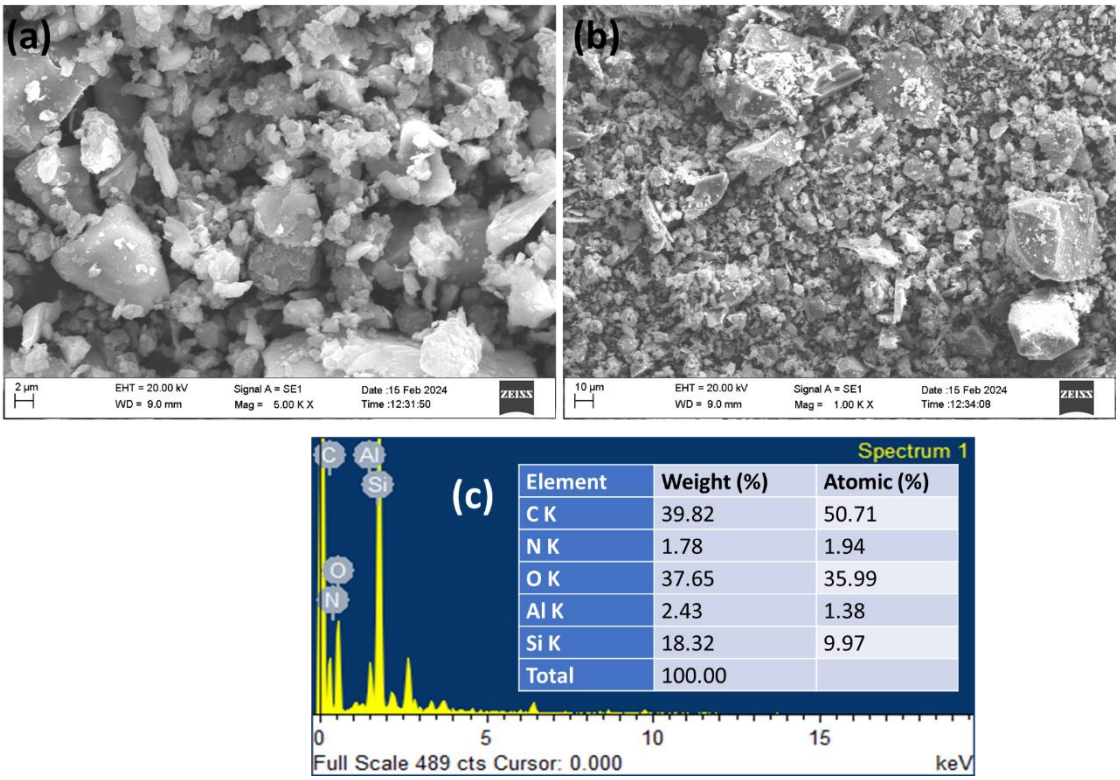

Figure 3.7 SEM image and EDAX of GS/PANI composite material

3.5.3 Powder XRD of GS and GS/PANI composite material

It is possible to obtain mineralogical and chemical composition information of sand by X-ray diffraction analysis. XRD is an excellent method for crystalline combination analysis, meanwhile every constituent of the blend gives its characteristic pattern individualistically of the others, making it possible to identify the various components by unravelling their superimposed patterns. Altitude and sharpness of the XRD peak is a quantification of the mineral and extent of crystallinity. The XRD pattern of Ganga sand (Figure 3.6 a) shows the presence of high quantity of highly crystalline quartz form of silica. There is marked difference observed in the XRD pattern of GS (Figure 3.6 a) and that of the GS/PANI composite (Figure 3.6 b) and it clearly indicated that there is surface modification of sand due to PANI deposition. The detailed XRD analysis of GS and GS/PANI composite is a matter of further research.

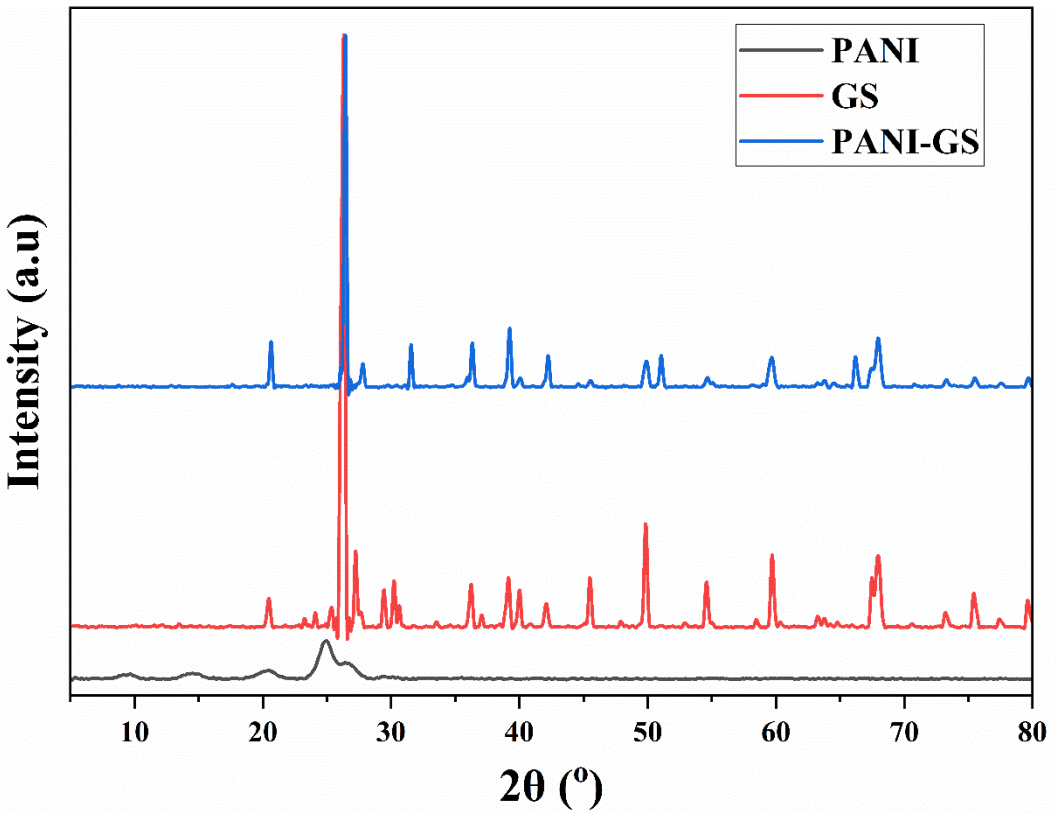

Figure 3.8 Powder XRD pattern of GS, PANI, and GS/PANI composite material

3.5.4 CHN elemental analysis of GS and GS/PANI composite material

C, H, N, elemental analysis of GS and GS/PANI composite provide the strong evidence of deposition of PANI over sand particles. There is marked increase in % of carbon nitrogen and hydrogen content shown in Table 3.1. Polymer deposition over sand may be higher when taking more aniline monomer. We had taken small ratio of aniline/sand so that there is more modification of sand surface. On using larger amount of aniline, the processing cost of material will go up for preparing composite material.

Table 3.1 C, H, N elemental analysis

Adsorbent	% C	% H	% N
GS	0.34	0.10	0.005
GS/PANI Composite	18.2	1.2	3.61

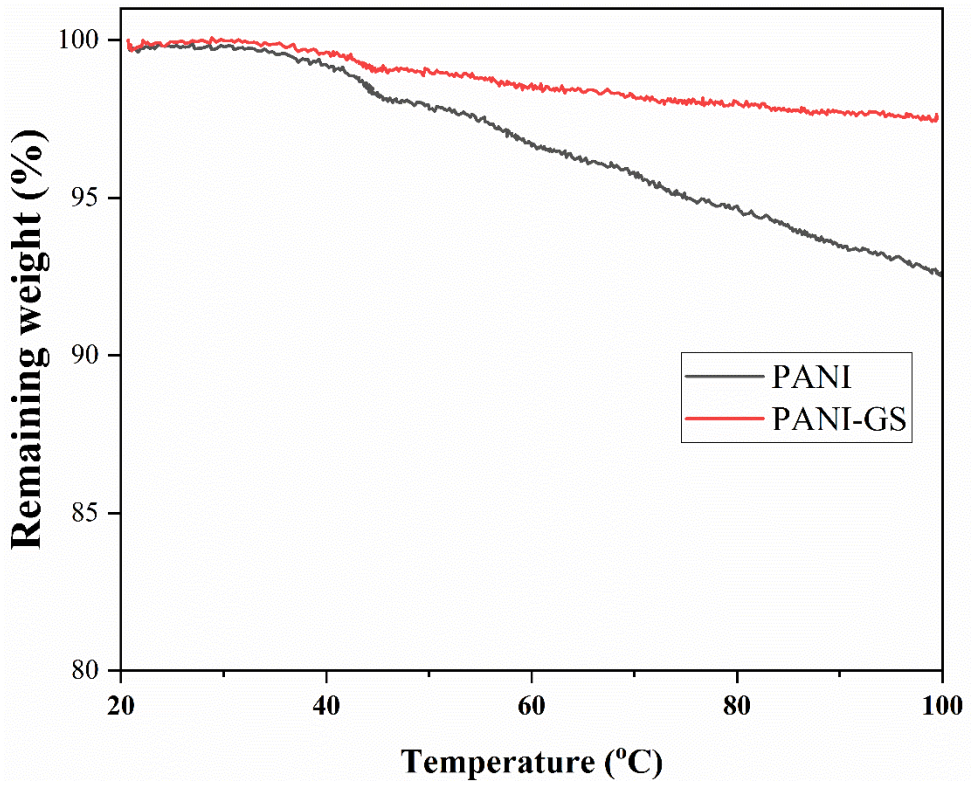

Figure 3.9 TGA plots of GS, and GS/PANI composite material

Figure 3.9 displays the TGA data, which were used to examine the mass losses of the produced materials as a function of temperature. The TGA data indicate that the PANI and GS/PANI composite have a negligible % mass loss of 7.5% between 20 ∘C and 100 ∘C. Such mass. Since the temperature during the adsorption process is not very high, the synthesized material will have sufficient operability over the application's temperature range.

3.5.5 FTIR of GS and GS/PANI composite material

The infrared spectra of the GS and GS/PANI composite were recorded as KBr discs using Perkin-Elmer spectrophotometer model 783 in the range of 4000-200 cm^{-1}. FTIR spectrum of GS and GS/PANI composites is shown in (Figures 3.10). Spectra of Ganga sand contains the bands corresponding stretching and bending vibrations of quartz (1081 cm^{-1}, 778 cm^{-1}, 690 cm^{-1}, 460 cm^{-1}), Si–O in-plane and out-of-plane stretching vibrations at around 1035 cm^{-1} and around 1081 cm^{-1}. The empirical formula corresponding to Polyaniline is $C_{24}H_{20}N_4$. The details of Polyaniline FTIR have been reported in the literature extensively. Broad peak at around 3500 cm^{-1} is attributed for the N–H stretching, at around 3200 cm^{-1} for the O-H stretch of water molecules physiosorbed at the PANI backbone, at around 1560 cm^{-1} is due to the quinonoid structure of PANI, sharp peak at around 1480 cm^{-1} is corresponding to the benzenoid structure of PANI, at around 800 cm^{-1} is evidence for C–H out of plane bending vibration. Strong Bands at frequency 3400 cm^{-1} indicate the deposition of PANI over sand grains. Very small amount of PANI deposited over sand surface as a result we observed weak peaks (characteristics of PANI) in GS/PANI composite. Intensity of peaks increases around 1500 cm^{-1} and 1600 cm^{-1} is due to the quinoid and benzoid units of PANI.

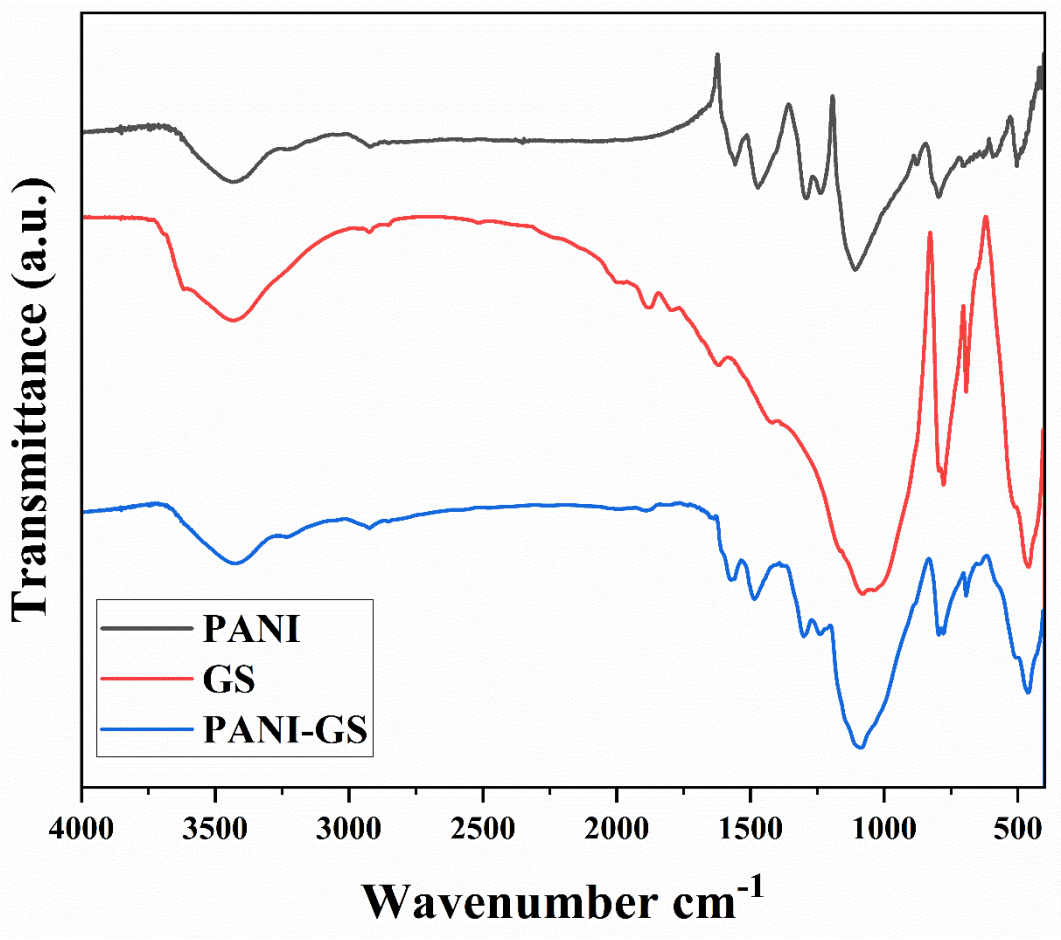

Figure 3.10 FTIR spectrum of GS, PANI and GS/PANI composite material

3.5.6 Adsorption of MB dye and DXN antibiotic on GS/PANI composite

We selected MB dye and DXN antibiotic for showing the suitability of GS/PANI composite as an effective low-cost adsorbent material. Effect of parameters such as preliminary MB dye and DXN antibiotic concentration, pH of the MB dye and DXN antibiotic solution, adsorbent dosage, contact time was studied for determining the adsorption behaviour of the synthesized adsorbent.

3.5.7 Effect of adsorbent dose

To eliminate MB dye and DXN antibiotic with sugarcane bagasse, the effect of adsorbent dose was studied keeping other parameters constant (Figure 3.11). The removal efficiency of MB dye and DXN antibiotic increased with increase in adsorbent dose from 0 to 12 g/L. The removal efficiency also showed an increment with increasing adsorbent dose was attributed to

increased accessibility of adsorption sites even though the increase in the removal efficiency of dyes showed great difference between each other this was according to the capability of the respective dye in accordance to the sugarcane bagasse. As observed from (Figure 3.11) the MB dye showed better adsorption with GS/PANI composite material as the adsorbent dose whereas DXN antibiotic showed lower adsorption with increasing adsorbent dose. Whereas the adsorption capacity decreases with increase in dose that is it decreases with increase in removal efficiency as well. The maximum adsorption capacity was shown by MB dye (99.2%). The least adsorption capacity is depicted by DXN antibiotic (86.5%).

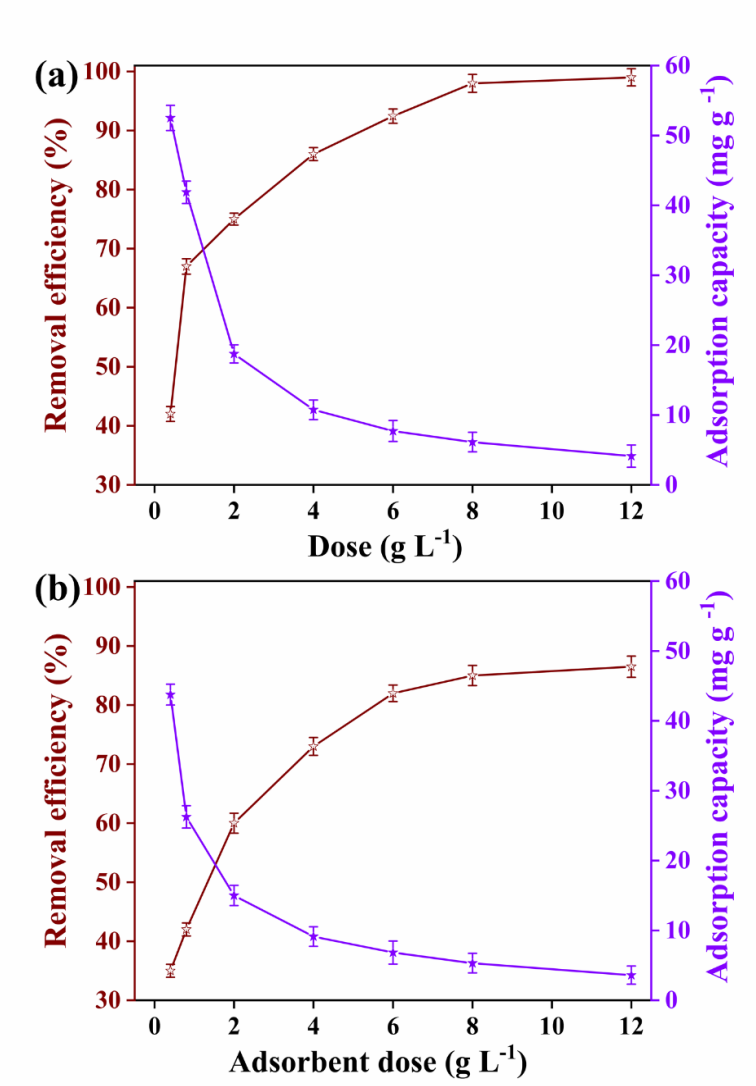

Figure 3.11 Removal efficacy of (a) MB dye and (b) DXN antibiotic using GS/PANI composite material with variable adsorbent dose. (Initial dye concentrations: 50 ppm, contact time: 120 min, and pH: 12 for MB and 7 for DXN)

3.5.8 Effect of pH

To study the consequence of MB dye and DXN antibiotic solution pH on the adsorption removal efficacy of GS/PANI composite material adsorbent, the pH of the solution was varied from 2 to 12, while keeping other parameters fixed. With increase in MB dye solution pH the removal efficacy amplified from 40.1 % to 99.5 % with the extreme elimination efficacy at 10 pH (Figure 3.12). In the similar trend with increase in DXN antibiotic solution pH, the removal efficacy also increased from 38.3% to 68% on. This increase in elimination efficacy can be clarified by the negative charge existing on the GS/PANI composite material a positive charge on MB dye and negative charge on DXN antibiotic, Chiao et al. (2020), Chen et al. (2017). This surface charges were responsible for an attractive interaction between MB dye and GS/PANI composite material adsorbent results in rise of the removal efficacy.

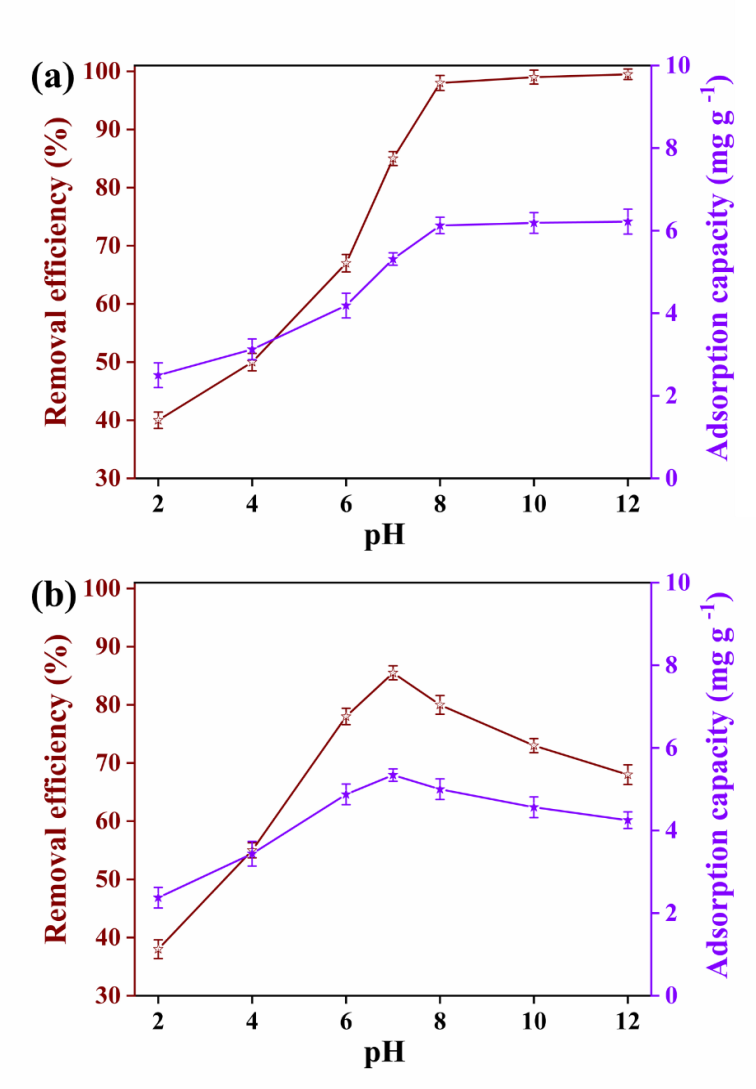

Figure 3.12 Removal efficacy of (a) MB dye and (b) DXN antibiotic using GS/PANI composite material with variable pH. (Adsorbent dose: 8 g L^{-1}, initial dye concentrations: 50 ppm, contact time: 120 min)

3.5.9 Effect of contact time

The influence contact time between the GS/PANI composite material adsorbent and MB dye and DXN antibiotic removal efficacy for adsorption was examined with variable contact time while keeping other parameters fixed. The removal efficacy increased speedily with increase in contact time of the adsorbent and later some point of time it the curve become plateau (Figure 3.13). The increases in removal efficacy were attributed to the fact that initially the availability

of additional adsorption active sites, and as the adsorption procedure passes the active number of sites decreases (as adsorbent dose was fixed), hence the curve become plateau. The highest removal efficiency of MB was 98.07 % at 180 min after which the removal efficacy and adsorption capacity plots become plateau. The similar observations also seen in other studies, Geng et al. (2018).

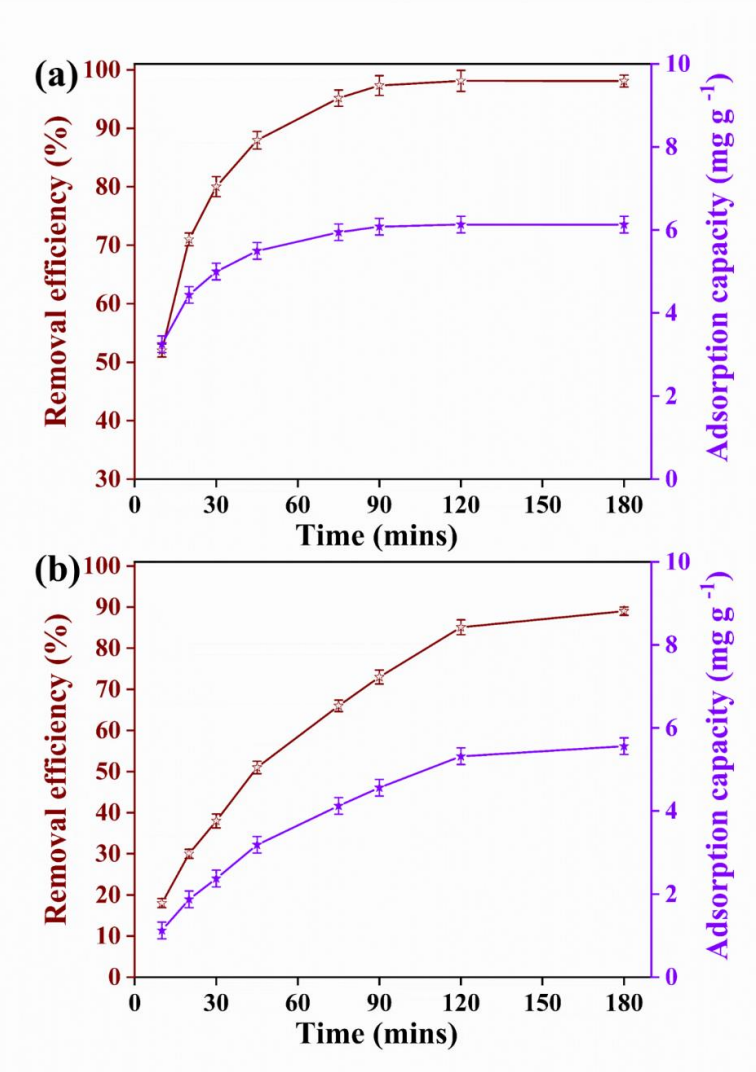

Figure 3.13 Removal efficacy of (a) MB dye and (b) DXN antibiotic using GS/PANI composite material with variable contact time. (Adsorbent dose: 8 g L^{-1}, initial dye concentrations: 50 ppm, and pH: 12 for MB and 7 for DXN)

3.5.10 Effect of the initial dye concentration

The influence preliminary concentration of MB dye and DXN antibiotic on removal efficacy was examined keeping other parameters fixed. The removal efficiency reduced as the preliminary concentration rose (Figure 3.14). The removal efficacy diminished was most likely due to increased contact of dye with available active sites on GS/PANI composite material adsorbent. When initial concentration of MB dye increased from 10 to 120 ppm, the removal efficacy showed a reduction 99.2% to 55.1%. The removal efficacy decreased also due to static adsorbent dose as concentration dye molecules increased but the adsorbent sites was fixed therefore the GS/PANI composite material adsorbent cannot holds the others dye molecules, Jahan et al. (2020), Liu et al. (2019).

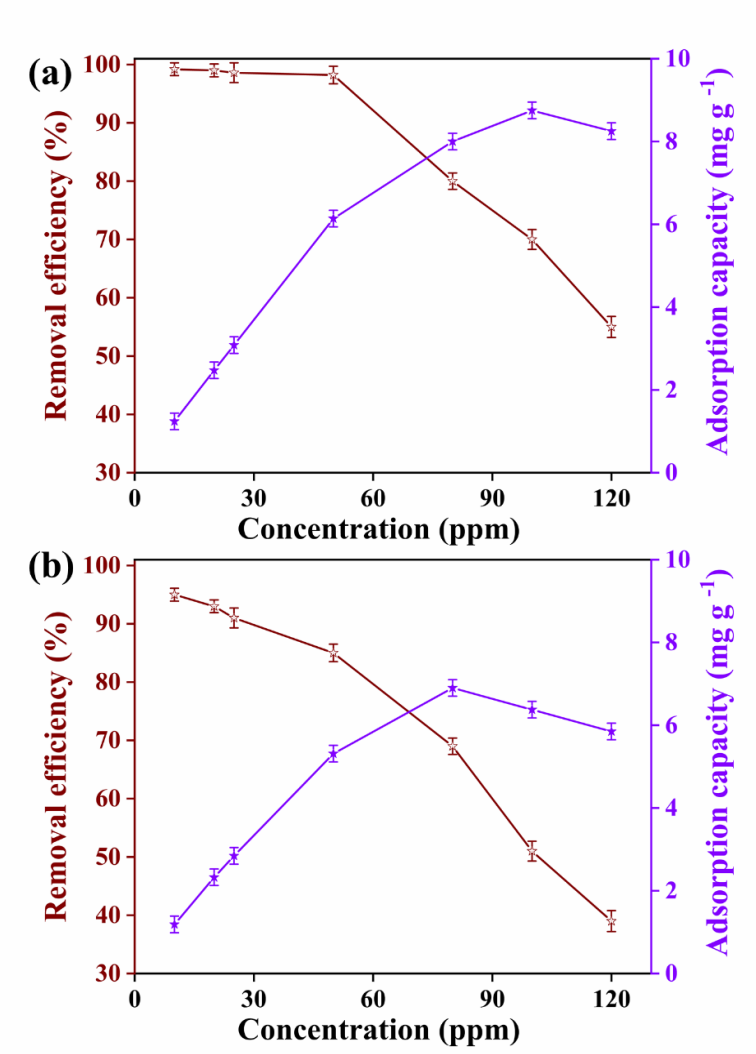

Figure 3.14 Removal efficacy of **(a)** MB dye and **(b)** DXN antibiotic using GS/PANI composite material with variable initial concentrations of MB dye. (Adsorbent dose: 8 g L^{-1}, contact time: 120 min, and pH: 12 for MB and 7 for DXN)

3.6 Adsorption kinetics and isotherm models

Optimization of contact time is important for the adsorption examination, to confirm complete equilibrium between the MB dye and DXN antibiotic and GS/PANI composite material adsorbent. The pseudo-first-order (PFO) and pseudo-second-order (PSO) models adsorption kinetics were investigated to propose a plausible kinetic mechanism. Table 3.2 depicts the different parameter of the PFO and PSO adoption kinetics for adsorption of MB dye and DXN antibiotic on GS/PANI composite material adsorbent. The correlation coefficient (R^2) value for PFO and PSO model were 0.9012 and 0.9992, respectively for MB dye adsorption on GS/PANI composite material. The R^2 value for PFO and PSO model were 0.6971 and 0.9932, respectively for DXN antibiotic adsorption on GS/PANI composite material. The R^2 value for PFO was far than unity compared to PSO model indicating the PSO linear second-order model fitting for the adsorption of MB dye GS/PANI composite material adsorbent. The PSO model fitting established the adsorption was of chemical nature, Kuwer et al. (2021). These values of PSO model compared to the PFO model was due to the smaller difference in between the experimental and theoretical values for PSO and PFO model (Figure 3.15).

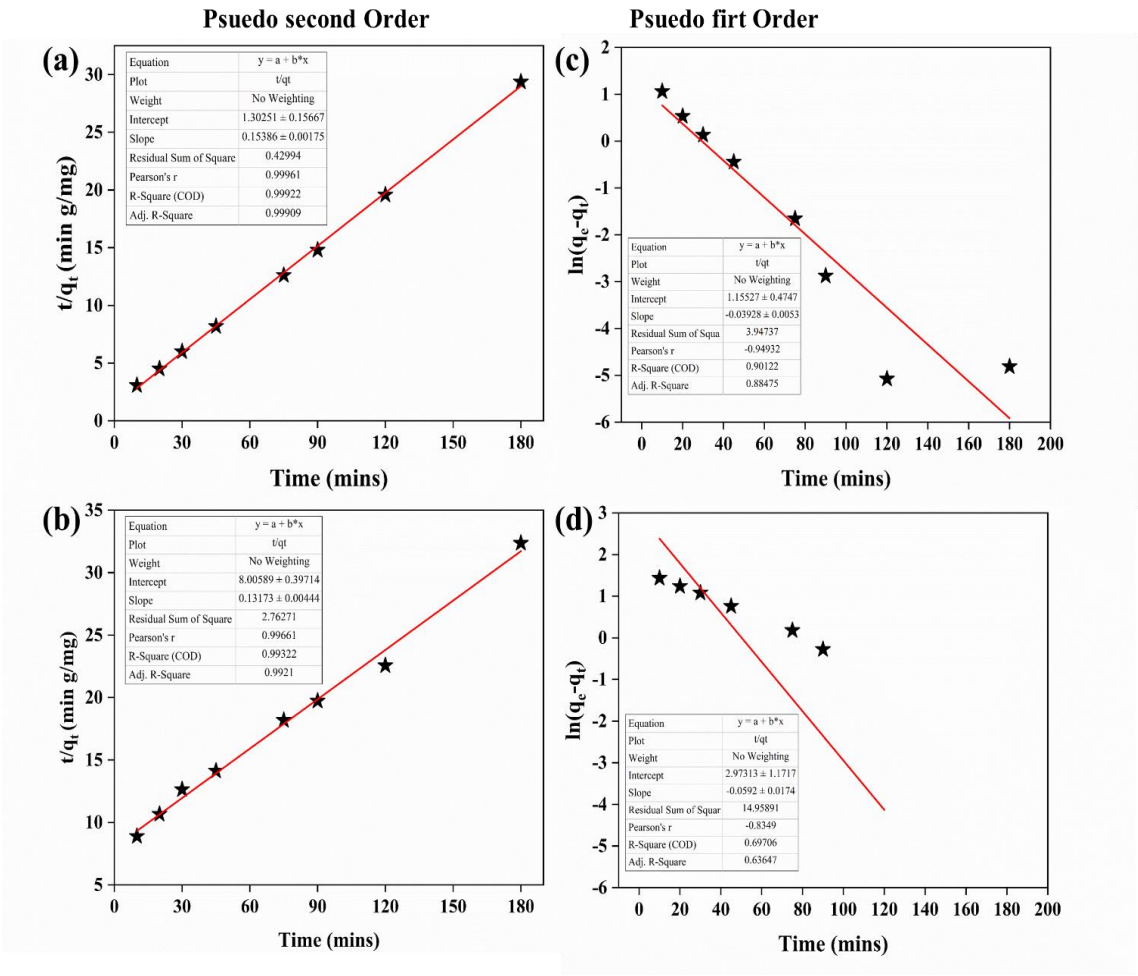

Figure 3.15 Linear form of kinetic isotherms PFO and PSO model fittings

Table 3.2 PFO and PSO kinetics' parameter for dye adsorption on GS/PANI composite material

	MB		**DXN**	
	PSO	**PFO**	**PSO**	**PFO**
Intercept	1.303	1.155	8.006	2.973
Slope	0.254	-0.039	0.132	-0.059
q_e **(mg g^{-1})**	3.937008	3.174023	7.575758	19.55048
$k1$ **(min^{-1})**	0.049513	-0.00022	0.002176	-0.00033
R^2	0.999	0.993	0.901	0.697

Two adsorption isotherm (Freundlich and Langmuir) was examined for adsorption of MB dye and DXN antibiotic on GS/PANI composite material adsorbent in the current chpter. The regression coefficient (R^2), reduced chi-square, and residual sum of the square were assessed to distinguish between two isotherm models (Table 3.3). The R^2 value was close to unity in the case for the Langmuir model (Freundlich: 0.8405 and Langmuir: 0.9933) for MB dye adsorption on GS/PANI composite material adsorbent. R^2 value was get suitable show fitting with the Langmuir isotherm model for MB dye adsorption on GS/PANI composite material adsorbent. If value of K_L is in between 0 and 1, the system is considered suitable for adsorption purpose, for the present study value of n was 18 indicating the GS/PANI composite material adsorbent are suitable for the MB dye adsorption. Moreover, the experimental data and predicted results obtained for the MB dye adsorption on GS/PANI composite material adsorbent were found in close correlation (R^2 = 0.9933) making this model applicable for the present chapter. A typical Langmuir isotherm shows a characteristic horizontal asymptote indicating saturation after the monolayer adsorption. This shown that the adsorption mechanism of dyes on GS/PANI composite material adsorbent was chemisorption Bangari et al. (2021). The closeness of experimental and predicted data points was also examined (Figure 3.16).

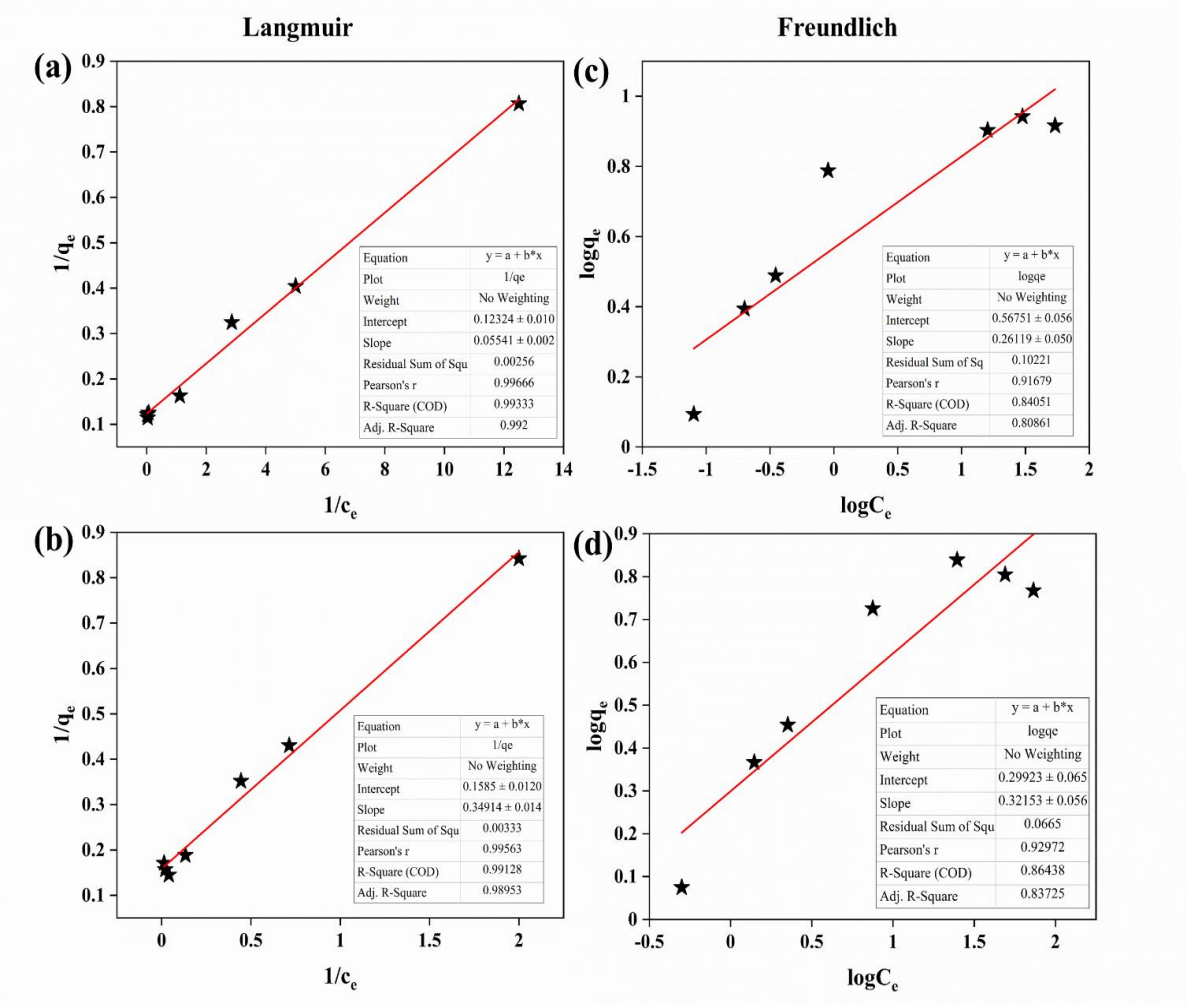

Figure 3.16 Linear form of adsorption isotherms Freundlich and Langmuir model fittings

Table 3.3 Freundlich and Langmuir isotherm's parameter for dye adsorption on GS/PANI composite material

	MB		**DXN**	
	Freundlich	**Langmuir**	**Freundlich**	**Langmuir**
Intercept	0.5675	0.1232	0.299	0.158
Slope	0.2612	0.0554	0.322	0.349
K	1.763852	146.5141	1.34851	18.135
n	3.828484	-	3.10559	-
R^2	0.841	0.993	0.864	0.991

3.7 Conclusion

Elimination of MB dye from aqueous solution onto sand based composite material surface was carried out at room temperature. The optimum experimental parameters for the removal of MB by GS/PANI composite material are: adsorbent dose: 8 g/L, initial dye concentration 50 ppm, contact time 120 minute: optimum pH 12. The optimum experimental parameters for the removal of doxycycline by GS/PANI composite material are: adsorbent dose: 8 g/L, initial concentration 50 ppm, contact time 120 minute: optimum pH 7. GS/PANI composite material is better adsorbent than pure GS. From the adsorption isotherm Langmuir & Freundlich the value of R^2 is more than Freundlich adsorption isotherm & Pseudo first-order-model observed to fit well with the data. The removal efficiency of PANI sand composite material is quite good and said composite material study is new in term of adsorption study.

3.8 References

Abdulsahib, W. K., Ganduh, S. H., Mahdi, M. A., & Jasim, L. S. (2020). Adsorptive removal of doxycycline from aqueous solution using graphene oxide/hydrogel composite. International Journal of Applied Pharmaceutics, 100–106. https://doi.org/10.22159/ijap.2020v12i6.39118

Ahmed, T., Noor, W., Faruk, O., Bhoumick, M. C., & Uddin, M. T. (2018). Removal of methylene blue (MB) from waste water by adsorption on jackfruit leaf powder (JLP) in continuously stirred tank reactor. Journal of Physics Conference Series, 1086, 012012. https://doi.org/10.1088/1742-6596/1086/1/012012

Ali, M. M. M., & Ahmed, M. J. (2017). Adsorption behavior of doxycycline antibiotic on NaY zeolite from wheat (Triticum aestivum) straws ash. Journal of the Taiwan Institute of Chemical Engineers, 81, 218–224. https://doi.org/10.1016/j.jtice.2017.10.026

Aniagor, C. O., Igwegbe, C. A., Ighalo, J. O., & Oba, S. N. (2021). Adsorption of doxycycline

from aqueous media: A review. Journal of Molecular Liquids, 334, 116124. https://doi.org/10.1016/j.molliq.2021.116124

Ashik, A. A., Rahman, M. A., Halder, D., & Hossain, M. M. (2023). Removal of methylene blue from aqueous solution by coconut coir dust as a low-cost adsorbent. Applied Water Science, 13(3). https://doi.org/10.1007/s13201-023-01887-5

Bai, B., Xu, X., Li, C., Xing, J., Wang, H., & Suo, Y. (2018). Magnetic Fe_3O_4@Chitosan Carbon Microbeads: Removal of Doxycycline from Aqueous Solutions through a Fixed Bed via Sequential Adsorption and Heterogeneous Fenton-Like Regeneration. Journal of Nanomaterials, 2018, 1–14. https://doi.org/10.1155/2018/5296410

Bangari, R. S., Yadav, A., Awasthi, P., & Sinha, N. (2021). Experimental and theoretical analysis of simultaneous removal of methylene blue and tetracycline using boron nitride nanosheets as adsorbent. Colloids and Surfaces a Physicochemical and Engineering Aspects, 634, 127943. https://doi.org/10.1016/j.colsurfa.2021.127943

Calimli, M. H., Nas, M. S., Burhan, H., Mustafov, S. D., Demirbas, O., & Sen, F. (2020). Preparation, characterization and adsorption kinetics of methylene blue dye in reduced-graphene oxide supported nanoadsorbents. Journal of Molecular Liquids, 309, 113171. https://doi.org/10.1016/j.molliq.2020.113171

Chen, M., Xiao, C., Wang, C., & Liu, H. (2017). Study on the structural design and performance of novel braid-reinforced and thermostable poly(m-phenylene isophthalamide) hollow fiber membranes. RSC Advances, 7(33), 20327–20335. https://doi.org/10.1039/c7ra01171g

Chiao, Y., Chen, S., Sivakumar, M., Ang, M. B. M. Y., Patra, T., Almodovar, J., Wickramasinghe, S. R., Hung, W., & Lai, J. (2020). Zwitterionic Polymer Brush Grafted on Polyvinylidene Difluoride Membrane Promoting Enhanced Ultrafiltration Performance with Augmented Antifouling Property. Polymers, 12(6), 1303. https://doi.org/10.3390/polym12061303

Fakher, S., & Imqam, A. (2019). A review of carbon dioxide adsorption to unconventional shale rocks methodology, measurement, and calculation. SN Applied Sciences, 2(1). https://doi.org/10.1007/s42452-019-1810-8

Gautam, V., Singh, K. P., & Yadav, V. L. (2017). Multicomponent Template Effects—Preparation of highly porous polyaniline nanorods using crude lemon juice and its application for selective detection of catechol. ACS Sustainable Chemistry & Engineering, 6(2), 2256–2268. https://doi.org/10.1021/acssuschemeng.7b03705

Gautam, V., Singh, K. P., & Yadav, V. L. (2018). Preparation and characterization of green-nano-composite material based on polyaniline, multiwalled carbon nano tubes and carboxymethyl cellulose: For electrochemical sensor applications. Carbohydrate Polymers, 189, 218–228. https://doi.org/10.1016/j.carbpol.2018.02.029

Geng, Y., Zhang, J., Zhou, J., & Lei, J. (2018). Study on adsorption of methylene blue by a novel composite material of TiO2 and alum sludge. RSC Advances, 8(57), 32799–32807. https://doi.org/10.1039/c8ra05946b

Ghaemi, M., & Absalan, G. (2014). Fast removal and determination of doxycycline in water samples and honey by Fe_3O_4 magnetic nanoparticles. Journal of the Iranian Chemical Society, 12(1), 1–7. https://doi.org/10.1007/s13738-014-0450-6

Hasanova, M. K. (2021). Study of Sorption Kinetics of Doxycycline on pH Sensitive Hydrogel-based Graft Copolymers of Chitosan/Arabinogalactan/ Gummiarabic with Vinyl Monomers. Oriental Journal of Chemistry, 37(6), 1350–1358. https://doi.org/10.13005/ojc/370612

Huang, D., Zhang, Y., Zhang, J., Wang, H., Wang, M., Wu, C., Cheng, D., Chi, Y., & Zhao, Z. (2019). The synergetic effect of a structure-engineered mesoporous SiO2–ZnO composite for doxycycline adsorption. RSC Advances, 9(66), 38772–38782. https://doi.org/10.1039/c9ra08106b

Jahan, K., Tyeb, S., Kumar, N., & Verma, V. (2020). Bacterial Cellulose-Polyaniline Porous Mat for Removal of Methyl Orange and Bacterial Pathogens from Potable Water. Journal of Polymers and the Environment, 29(4), 1257–1270. https://doi.org/10.1007/s10924-020-01947-w

Khan, M., Ali, S. W., Shahadat, M., & Sagadevan, S. (2022). Applications of polyaniline-impregnated silica gel-based nanocomposites in wastewater treatment as an efficient adsorbent of some important organic dyes. Green Processing and Synthesis, 11(1), 617–630. https://doi.org/10.1515/gps-2022-0063

Kurniawati, D., Bahrizal, N., Sari, T. K., Adella, F., & Sy, S. (2021). Effect of Contact Time Adsorption of Rhodamine B, Methyl Orange and Methylene Blue Colours on Langsat Shell with Batch Methods. Journal of Physics Conference Series, 1788(1), 012008. https://doi.org/10.1088/1742-6596/1788/1/012008

Kuwer, P., Yadav, A., & Labhasetwar, P. K. (2021). Adsorption of cupric, cadmium and cobalt ions from the aqueous stream using the composite of iron(II,III) oxide and zeolitic imidazole framework-8. Water Science & Technology, 84(9), 2288–2303. https://doi.org/10.2166/wst.2021.452

Lin, J., & Wang, L. (2009). Comparison between linear and non-linear forms of pseudo-first-order and pseudo-second-order adsorption kinetic models for the removal of methylene blue by activated carbon. Frontiers of Environmental Science & Engineering in China, 3(3), 320–324. https://doi.org/10.1007/s11783-009-0030-7

Liu, Y., Huang, Y., Xiao, A., Qiu, H., & Liu, L. (2019). Preparation of magnetic FE3O4/MIL-88A nanocomposite and its adsorption properties for bromophenol blue dye in aqueous solution. Nanomaterials, 9(1), 51. https://doi.org/10.3390/nano9010051

Mate, C. J., & Mishra, S. (2020). Synthesis of borax cross-linked Jhingan gum hydrogel for remediation of Remazol Brilliant Blue R (RBBR) dye from water: Adsorption isotherm,

kinetic, thermodynamic and biodegradation studies. International Journal of Biological Macromolecules, 151, 677–690. https://doi.org/10.1016/j.ijbiomac.2020.02.192

Othman, N. H., Alias, N. H., Shahruddin, M. Z., Bakar, N. F. A., Him, N. R. N., & Lau, W. J. (2018). Adsorption kinetics of methylene blue dyes onto magnetic graphene oxide. Journal of Environmental Chemical Engineering, 6(2), 2803–2811. https://doi.org/10.1016/j.jece.2018.04.024

Rahman, N., & Varshney, P. (2021). Effective removal of doxycycline from aqueous solution using CuO nanoparticles decorated poly(2-acrylamido-2-methyl-1-propanesulfonic acid)/chitosan. Environmental Science and Pollution Research, 28(32), 43599–43617. https://doi.org/10.1007/s11356-021-13584-4

Ramutshatsha-Makhwedzha, D., Mavhungu, A., Moropeng, M. L., & Mbaya, R. (2022). Activated carbon derived from waste orange and lemon peels for the adsorption of methyl orange and methylene blue dyes from wastewater. Heliyon, 8(8), e09930. https://doi.org/10.1016/j.heliyon.2022.e09930

Sahu, N., Rawat, S., Singh, J., Karri, R. R., Lee, S., Choi, J., & Koduru, J. R. (2019). Process Optimization and Modeling of Methylene Blue Adsorption Using Zero-Valent Iron Nanoparticles Synthesized from Sweet Lime Pulp. Applied Sciences, 9(23), 5112. https://doi.org/10.3390/app9235112

Saxena, M., Kushwaha, J. P., Kulshreshtha, S., Kaur, G., & Singh, N. (2022). Doxycycline Adsorptive Interaction with Mesoporous MCM-41: Kinetic and Isotherm Modelling with Thermodynamics. Chemistry Africa, 5(4), 1055–1068. https://doi.org/10.1007/s42250-022-00365-w

Wei, J., Liu, Y., Li, J., Zhu, Y., Yu, H., & Peng, Y. (2019). Adsorption and co-adsorption of tetracycline and doxycycline by one-step synthesized iron loaded sludge biochar. Chemosphere, 236, 124254. https://doi.org/10.1016/j.chemosphere.2019.06.224

Xiong, W., Zeng, Z., Li, X., Zeng, G., Xiao, R., Yang, Z., Xu, H., Chen, H., Cao, J., Zhou, C., & Qin, L. (2019). Ni-doped MIL-53(Fe) nanoparticles for optimized doxycycline removal by using response surface methodology from aqueous solution. Chemosphere, 232, 186–194. https://doi.org/10.1016/j.chemosphere.2019.05.184

Xu, X., Ma, W., An, B., Zhou, K., Mi, K., Huo, M., Liu, H., Wang, H., Liu, Z., Cheng, G., & Huang, L. (2021). Adsorption/desorption and degradation of doxycycline in three agricultural soils. Ecotoxicology and Environmental Safety, 224, 112675. https://doi.org/10.1016/j.ecoenv.2021.112675

Yu, Y., Chen, D., Xu, W., Fang, J., Sun, J., Liu, Z., Chen, Y., Liang, Y., & Fang, Z. (2021). Synergistic adsorption-photocatalytic degradation of different antibiotics in seawater by a porous g-C3N4/calcined-LDH and its application in synthetic mariculture wastewater. Journal of Hazardous Materials, 416, 126183. https://doi.org/10.1016/j.jhazmat.2021.126183

Zaidi, S., Chaabane, T., Sivasankar, V., Darchen, A., Maachi, R., Msagati, T., & Prabhakaran, M. (2016). Performance efficiency of electro-coagulation coupled electro-flotation process (EC-EF) versus adsorption process in doxycycline removal from aqueous solutions. Process Safety and Environmental Protection, 102, 450–461. https://doi.org/10.1016/j.psep.2016.04.013

Zeng, Z., Tan, X., Liu, Y., Tian, S., Zeng, G., Jiang, L., Liu, S., Li, J., Liu, N., & Yin, Z. (2018). Comprehensive adsorption studies of doxycycline and ciprofloxacin antibiotics by Biochars prepared at different temperatures. Frontiers in Chemistry, 6. https://doi.org/10.3389/fchem.2018.00080